NASA TECHNICAL NOTE

NASA TN D-2853

NASA TN D-2853

AERODYNAMIC CHARACTERISTICS OF A FAMILY OF MULTISTAGE MISSILES AT A MACH NUMBER OF 6.0

by E. Leon Morrisette and David J. Romeo

Langley Research Center

Langley Station, Hampton, Va.

NATIONAL AERONAUTICS AND SPACE ADMINISTRATION • WASHINGTON, D. C. • JUNE 1965

NASA TN D-2853

AERODYNAMIC CHARACTERISTICS OF A FAMILY OF MULTISTAGE MISSILES AT A MACH NUMBER OF 6.0

By E. Leon Morrisette and David J. Romeo

Langley Research Center
Langley Station, Hampton, Va.

NATIONAL AERONAUTICS AND SPACE ADMINISTRATION

For sale by the Clearinghouse for Federal Scientific and Technical Information
Springfield, Virginia 22151 – Price $2.00

AERODYNAMIC CHARACTERISTICS OF A FAMILY OF MULTISTAGE MISSILES AT A MACH NUMBER OF 6.0

By E. Leon Morrisette and David J. Romeo
Langley Research Center

26643

SUMMARY

An investigation of the aerodynamic characteristics of a series of one-, two-, and three-stage missiles was conducted through an angle-of-attack range from about -2° to 15° at a Mach number of 6. Geometric variables considered were nose shape, flare size and shape, stage fineness ratio, and interstage diameter ratio. Experimentally determined values of axial-force, normal-force, and pitching-moment coefficients are compared with calculations based on Newtonian impact theory for a total of 46 configurations.

The theory was found to predict satisfactorily the effect of a change in design variables and angle of attack for those configurations without flow separation. In general, the predictions improved with increasing nose bluntness and stage fineness ratio and with decreasing interstage diameter ratio and number of stages.

The effects of variation of fineness ratio and interstage diameter ratio were strongly influenced by boundary-layer separation. Regions of flow separation on a relatively small third stage had large effects on the flow over the second stage and resulted in significant variation in the aerodynamic coefficients. Bow-shock impingement on interstage fairing resulted in large increases in axial force and significant deviation from the theory at high angles of attack.

author

INTRODUCTION

The aerodynamic characteristics of cone-cylinder and cone-cylinder-flare missile configurations have been studied in detail at supersonic Mach numbers (for example, refs. 1 to 4). However, data on multistage combinations at hypersonic Mach numbers are limited to specific design studies (for example, refs. 5 to 7) or configuration studies with few variables (for example, refs. 8 and 9) with the exception of a parametric study of two-stage configurations over a Mach number range of 1.5 to 5.0 as reported by Glover in reference 10.

It is the purpose of the study reported herein, therefore, to help fill the need for a systematic investigation of the parameters involved in multistage

missile design and to examine the applicability of the Newtonian impact calculations (see ref. 11) for prediction of the aerodynamic coefficients on these bodies at hypersonic Mach numbers.

This paper presents the experimental and calculated longitudinal force and moment coefficients of a series of one-, two-, and three-stage missiles through an angle-of-attack range of about -2° to 15° at a Mach number of 6.0. The effects of changes in fineness ratio, interstage diameter ratio, and nose shape are presented as well as the effect of stabilizing flares on a typical three-stage configuration.

SYMBOLS

The aerodynamic coefficients are referred to the body-axis system, and are based on the first-stage cross-sectional area of 2.404 sq in. and the first-stage diameter of 1.75 inches. The pitching-moment coefficients are given about the configuration center of volume, nose and stabilizing flare contribution being ignored.

A	cross-sectional area of first stage
C_A	axial-force coefficient, $\frac{\text{Axial force}}{qA}$
C_N	normal-force coefficient, $\frac{\text{Normal force}}{qA}$
C_m	pitching-moment coefficient, $\frac{\text{Pitching moment}}{qAd_F}$
C_{m_α}	pitching-moment-curve slope
d	diameter
l	length
q	free-stream dynamic pressure
x_{ref}	distance from model base to reference center measured in first-stage diameters
α	angle of attack
θ	fairing half-angle

Subscripts:

F	pertains to first stage
Fr	pertains to stabilizing flare
N	pertains to nose
S	pertains to second stage
T	pertains to third stage

Model component designations:

Fl	first-stage body (fineness ratio of 5)
Frl	14° half-angle conical flare (base diameter equal to $2.0d_F$)
Fr2	14° half-angle conical flare (base diameter equal to $1.5d_F$)
Fr3	45° half-angle conical flare (base diameter equal to $2.0d_F$)
Nl	20° sharp cone nose (radius equal to 0)
N2	20° blunted cone nose (radius equal to $0.125d_N$)
N3	20° blunted cone nose (radius equal to $0.375d_N$)
N4	hemisphere nose (radius equal to $0.500d_N$)
Sl,S2,...,S6	second-stage bodies (see fig. 1(b))
Tl,T2,...,T18	third-stage bodies (see fig. 1(b))

APPARATUS

Tunnel

This investigation was conducted in the Langley 20-inch Mach 6 tunnel. The tunnel is of the intermittent type and can operate with a stagnation pressure varying from approximately 7 to 38 atmospheres and a maximum stagnation temperature up to 600° F. The tunnel exhausts to the atmosphere through a diffuser that is augmented by an air ejector. The models were supported by a sting-mounted, strain-gage balance and the data were recorded on a high-speed digital-tape system. An optical system with a prism mounted in the first stage of the model was used to measure angle of attack of the model directly. More detailed descriptions of the tunnel and optical system are given in reference 12.

Models

The models used in the program are shown and described in figures 1 and 2. Figure 1(a) shows a typical complete configuration and figure 1(b) identifies the components that were used to make up the 46 different model configurations tested. The dimensions and geometric characteristics of the model components are given in figure 2. The configurations tested are identified by a combination of the component designations as given in figures 1(b) and 2. The range of geometric variables is summarized below.

Noses.- The four nose types tested were:

N1 - a 20° sharp cone
N2 - a 20° cone blunted with a radius equal to $0.125d_N$
N3 - a 20° cone blunted with a radius equal to $0.375d_N$
N4 - a hemisphere

Bodies.- The stages had fineness ratios of 2 and 5, and had their interstage fairings determined by the condition that the axial length of the fairing was equal to the diameter of the smaller stage.

Flares.- Conical flares Fr1 and Fr2 had half-angles of 14.0° and their base diameters were 2.0 or 1.5 times the first-stage base diameter. Conical flare Fr3 had a half-angle of 45.0° and its base diameter was 2.0 times the first-stage base diameter.

TESTS AND ACCURACY

Each configuration was tested through an angle-of-attack range from -2.5° to 14.5° at a free-stream Mach number of 6.0. The tunnel stagnation pressure was 390 psia, the stagnation temperature was 400° F, and the corresponding unit Reynolds number was approximately 7.4×10^6.

The maximum uncertainties in the force and moment coefficients for the individual test points due to the strain-gage balance were:

C_N . . . . . ±0.02
C_A . . . . . ±0.02
C_m . . . . . ±0.14

The stagnation pressures and base pressures were measured to an accuracy of ±2.5 psia and ±0.005 psia, respectively. The Mach number uncertainty was ±0.02 and the angle of attack could be set to an accuracy of ±0.10°. The axial-force coefficients were corrected to give coefficients corresponding to a base pressure equal to free-stream pressure.

THEORY

Newtonian impact theory (ref. 11) was used to predict the aerodynamic coefficients of all 46 of the tested configurations. The theory, as presented, is based on a maximum pressure coefficient of 2.0. In accounting for the "shadowing effect" of a stage on its trailing flare, an approximate linear boundary was used to calculate the coefficients, although the true shadowed portion of the flare was bounded by parabolic arcs. This resulted in lower axial-force coefficients and higher normal-force coefficients at low angle of attack than would have been obtained without considering the shadowing effect. The effect on C_m depended on the position of the flare relative to the model center of gravity. As the angle of attack increased, the flare became self-shadowing and the assumption of the linear boundary is exact.

RESULTS AND DISCUSSION

The data presented in figures 3 to 8 show the results of varying α on C_A, C_N, and C_m for the one-, two-, and three-stage models tested. Both experimental data and Newtonian impact theory are presented. The discussion is presented in the following order: effects of nose shape, effects of fineness ratio and interstage diameter ratio, and effects of flares on a three-stage configuration.

Effects of Nose Shape

The four nose shapes were tested on one-, two-, and three-stage vehicles. Each stage had a fineness ratio of 5. On the multistage configurations, each interstage diameter ratio was 1.6. Increasing the nose bluntness caused an increase in C_A and a decrease in C_N and C_m for all three types of configurations tested (figs. 3 to 5).

Newtonian theory gave excellent prediction of the axial-force coefficient for the blunt (N4 nose) single-stage body (fig. 3) but underestimated the values for the sharper cones. The value of C_A for the sharp cone could have been better estimated by oblique-shock theory. Newtonian theory predicts a substantial increase in C_A for a cone blunted to a radius of $0.125d_N$, but the experimental data show little difference in the values. The theory overestimates the increase of C_N with angle of attack for all the single-stage bodies. At the higher angles of attack, the calculated decrease in C_N due to blunting was approximately 20 percent, whereas the experimental values show a 30-percent decrease. The pitching-moment coefficients showed good agreement with theory throughout the angle-of-attack range.

As the number of stages increased, the relative nose size became smaller and the effects of nose bluntness variation diminished. Thus, the variation of the aerodynamic force coefficients due to nose blunting on the two-stage bodies (fig. 4) was less than that for the one-stage bodies (fig. 3). The theory was

in good agreement with the data for C_A and C_N. The agreement of theory and data improved for the three-stage vehicles (fig. 5) and the variation of force coefficients due to blunting was further decreased. The pitching-moment coefficients increased with increasing number of stages for both the theory and the data; however, the theory estimated the pitching-moment coefficients best for the one-stage missiles.

Effects of Fineness Ratio and Interstage Diameter Ratio

The aerodynamic coefficients (figs. 6 and 7) were well described by theory for configurations of high fineness ratios and small interstage diameter ratios. The agreement between theory and data was especially sensitive to interstage diameter ratio, and large discrepancies resulted for configurations having an interstage diameter ratio of 2.4. These discrepancies between theory and data resulted from large regions of laminar flow separation at low angles of attack, due to the large fairing angle or the close proximity of the flare to the bow shock at high angles of attack.

For the two-stage missiles shown in figure 6, an increase in the interstage diameter ratio $\left(d_F/d_S\right)$ from 1.2 to 1.6 is accompanied by a reduction in the value of C_A to below that of the single-stage missile (fig. 3); however, a further increase in d_F/d_S to 2.4 is accompanied by a greatly increased axial force. This reversal is a result of the increase in interstage flare angle with change in diameter ratio. The flare angles for the interstage diameter ratios of 1.2 and 1.6 are less than the nose-cone angle, whereas the flare angle for $d_F/d_S = 2.4$ is much greater than the nose-cone angle. In the low angle-of-attack range, the measured axial-force coefficients for two-stage missiles of large interstage diameter ratio were significantly lower than the predicted values. This overestimation was caused by regions of laminar separated flow on the interstage flares, which resulted in pressures lower than estimated on portions of the flares. The decrease in axial force was greatest for configuration N2-S5-F1 which has a fineness ratio $\left(l_S/d_S\right)$ of 5 and an interstage diameter ratio $\left(d_F/d_S\right)$ of 2.4 (fig. 6(b)). For this configuration the region of separation was large (see schlieren photograph, fig. 6(b)) and the axial-force coefficient at $\alpha = 0^\circ$ was only about one-half the value estimated by theory. There was also a region of separation on configuration N2-S6-F1 (fig. 6(a)) which had the same theoretical value of C_A at $\alpha = 0^\circ$, but the short length of the second stage $\left(l_S/d_S = 2\right)$ reduced the region of separation and lessened the decrease in axial force. As the angle of attack increased, the axial forces increased to values significantly higher than estimated for configurations with the large diameter ratios $\left(d_F/d_S = 2.4\right)$. This increase is caused by the interstage fairing moving close to the bow shock and thereby being placed in a region of high dynamic pressure, which results in higher than estimated pressure on the fairing. (See ref. 13.)

The combination of separation and bow-shock impingement results in a much greater increase in C_N with α than estimated for the configurations with large interstage diameter ratios. The separation causes higher pressures on

the cylindrical portions of the stages, and this increase in normal force is greater than the decrease due to the lowered fairing pressures. The values of C_N for the missiles with d_F/d_S of 1.2 and 1.6 are consistent with the theory, although the slopes of the C_N curves are slightly underestimated at $\alpha = 0^\circ$. Except for configurations having d_F/d_S of 1.2, the pitching-moment coefficients are underestimated at angles of attack greater than 12°. The pitching-moment curves for configurations with d_F/d_S of 2.4 are much higher than estimated at low angles of attack, as a result of the forward movement of the center of pressure and increased normal force due to separation.

The addition of a third stage to the two-stage configurations does not significantly alter the general patterns of the data (fig. 7). A notable exception to this occurs when a third stage of large interstage diameter ratio $\left(d_S/d_T = 1.6 \text{ or } 2.4\right)$ is on a configuration having a large first- to second-stage diameter ratio $\left(d_F/d_S = 2.4\right.$; figs. 7(a), 7(d), and 7(g)$\left.\right)$. The boundary layer is apparently tripped (made turbulent) by the third stage and there is little or no separation on the first- to second-stage fairing (see schlieren photograph, fig. 7(g)) and the resulting axial-force coefficients are close to the theoretical values. The forward movement of the center of pressure is more pronounced for the three-stage vehicles with d_S/d_T of 2.4; for example, configuration N2-T6-S1-F1 (fig. 7(f)) has a pitching-moment coefficient that is more than four times the theoretical value at $\alpha = 7^\circ$. The slope of the pitching-moment coefficient about the configuration center of volume was, in general, more positive than estimated by impact theory.

Although the prediction of the separation is beyond the scope of this investigation, significant improvements in calculation of the overall performance of these configurations would have been expected from the use of available separation criteria.

Effects of Flares

A typical three-stage configuration having a stage fineness ratio of 5, interstage diameter ratio of 1.6, and a nose of type N2 was tested to determine the effects of three flares (fig. 8). All three flares caused increases over basic body values in C_A and C_N and a decrease in C_m. Flares Fr1 and Fr2 with 14° half-angles had little or no flow separation and the data follow the theoretical curves closely, whereas flare Fr3 with a 45° half-angle caused extensive flow separation and the data varied considerably from the theory. Even with the flow separation, the axial-force coefficient for the configuration with flare Fr3 was large; this characteristic combined with the large normal force, resulted in a stable body $\left(C_{m_\alpha} \text{ negative}\right)$. Flare Fr1 also resulted in a stable configuration throughout the angle-of-attack range, whereas the configuration with Fr2 was stable only over a small angle-of-attack range (approximately 5° to 8°).

CONCLUDING REMARKS

An investigation of the aerodynamic characteristics of a series of one-, two-, and three-stage missiles was conducted at a Mach number of 6. Parameters considered were nose shape, flare size and shape, stage fineness ratio, interstage diameter ratio, and angle of attack. Experimentally determined values of axial-force, normal-force, and pitching-moment coefficients are compared with calculations based on Newtonian impact theory for a total of 46 configurations.

Newtonian impact theory was found to predict satisfactorily the effect of a change in design variables and angle of attack for those configurations without flow separation. In general, the predictions improved with increasing nose bluntness and stage fineness ratio and with decreasing interstage diameter ratio and number of stages.

Boundary-layer separation played a strong part in the result of variation of fineness ratio and interstage diameter ratio. Regions of flow separation on a relatively small third stage had large effects on the flow over the second stage and resulted in significant variations in the aerodynamic coefficients. Bow-shock impingement on interstage fairing resulted in large increases in axial force and significant deviation from theory at high angles of attack.

Langley Research Center,
National Aeronautics and Space Administration,
Langley Station, Hampton, Va., December 14, 1964.

REFERENCES

1. Jack, John R.; and Gould, Lawrence I.: Aerodynamics of Slender Bodies at Mach Number of 3.12 and Reynolds Numbers From 2×10^6 to 15×10^6. II - Aerodynamic Load Distributions of Series of Five Bodies Having Conical Noses and Cylindrical Afterbodies. NACA RM E52C10, 1952.

2. Dennis, David H.; and Cunningham, Bernard E.: Forces and Moments on Pointed and Blunt-Nosed Bodies of Revolution at Mach Numbers From 2.75 to 5.00. NACA RM A52E22, 1952.

3. Penland, Jim A.: Static Longitudinal Stability of a Missile Configuration With Various Nose Shapes and Flared Afterbodies at a Mach Number of 6.82. NASA TM X-274, 1960.

4. Penland, Jim A.: Aerodynamic Force Characteristics of a Series of Lifting Cone and Cone-Cylinder Configurations at a Mach Number of 6.83 and Angles of Attack Up to 130°. NASA TN D-840, 1961.

5. Canning, Thomas N.: Investigation of the Lift, Center of Pressure, and Drag of a Projectile at a Mach Number of 8.6 and a Reynolds Number of 17 Million. NACA RM A54H23a, 1954.

6. Lindsay, E. Earl; and Hillsamer, M. E.: Static Stability Characteristics of First and Second Stage Configurations of the Apollo Launch Vehicles at Supersonic and Hypersonic Mach Numbers. AEDC-TDR-63-26, U.S. Air Force (Contract AF 40(600)-1000), Feb. 1963.

7. Penland, Jim A.; and Fetterman, David E., Jr.: The Effects at a Mach Number of 6.86 of Drag Brakes on the Lift, Drag, and Pitching Moment of an Ogive Cylinder. NACA RM L55K23, 1955.

8. Penland, Jim A.; and Carroll, C. Maria: Static Longitudinal and Lateral Stability Parameters of Three Flared-Skirt Two-Stage Missile Configurations at a Mach Number of 6.86. NACA RM L57D15, 1957.

9. Turner, Kenneth L.; Shaw, David S.; and Enderson, Laurence W., Jr.: Static Stability and Separation Characteristics of a Two-Stage Rocket Configuration at Mach Numbers From 1.57 to 4.50. NASA TN D-188, 1960.

10. Glover, Warren G.: Investigation of the Aerodynamics of Basic Multistage Missile Shapes at Mach Numbers 1.5 to 5.0. AEDC-TR-61-3 (Contract No. AF 40(600)-800 S/A 24(61-73)), Arnold Eng. Dev. Center, July 1961.

11. Truitt, Robert Wesley: Hypersonic Aerodynamics. The Ronald Press Co., c.1959.

12. Ashby, George C., Jr.; and Fitzgerald, Paul E., Jr.: Longitudinal Stability and Control Characteristics of Missile Configurations Having Several Highly Swept Cruciform Fins and a Number of Trailing-Edge and Fin-Tip Controls at Mach Numbers From 2.21 to 6.01. NASA TM X-335, 1961.

13. Ashby, George C., Jr.; and Cary, Aubrey M., Jr.: A Parametric Study of the Aerodynamic Characteristics of Nose-Cylinder-Flare Bodies at a Mach Number of 6.0. NASA TN D-2854, 1965.

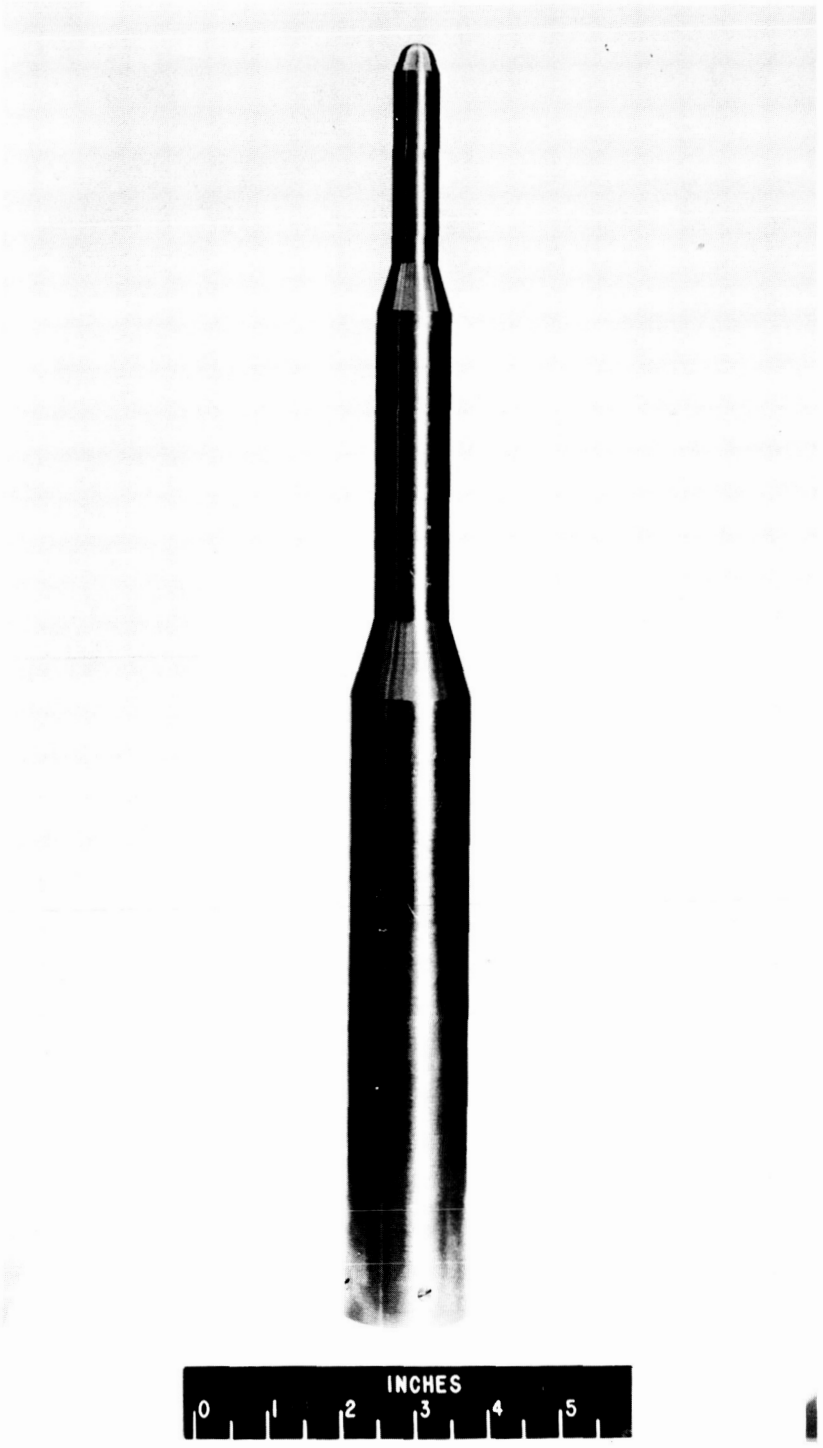

(a) Configuration N3-T9-S3-F1.

L-63-2169

Figure 1.- Model and components.

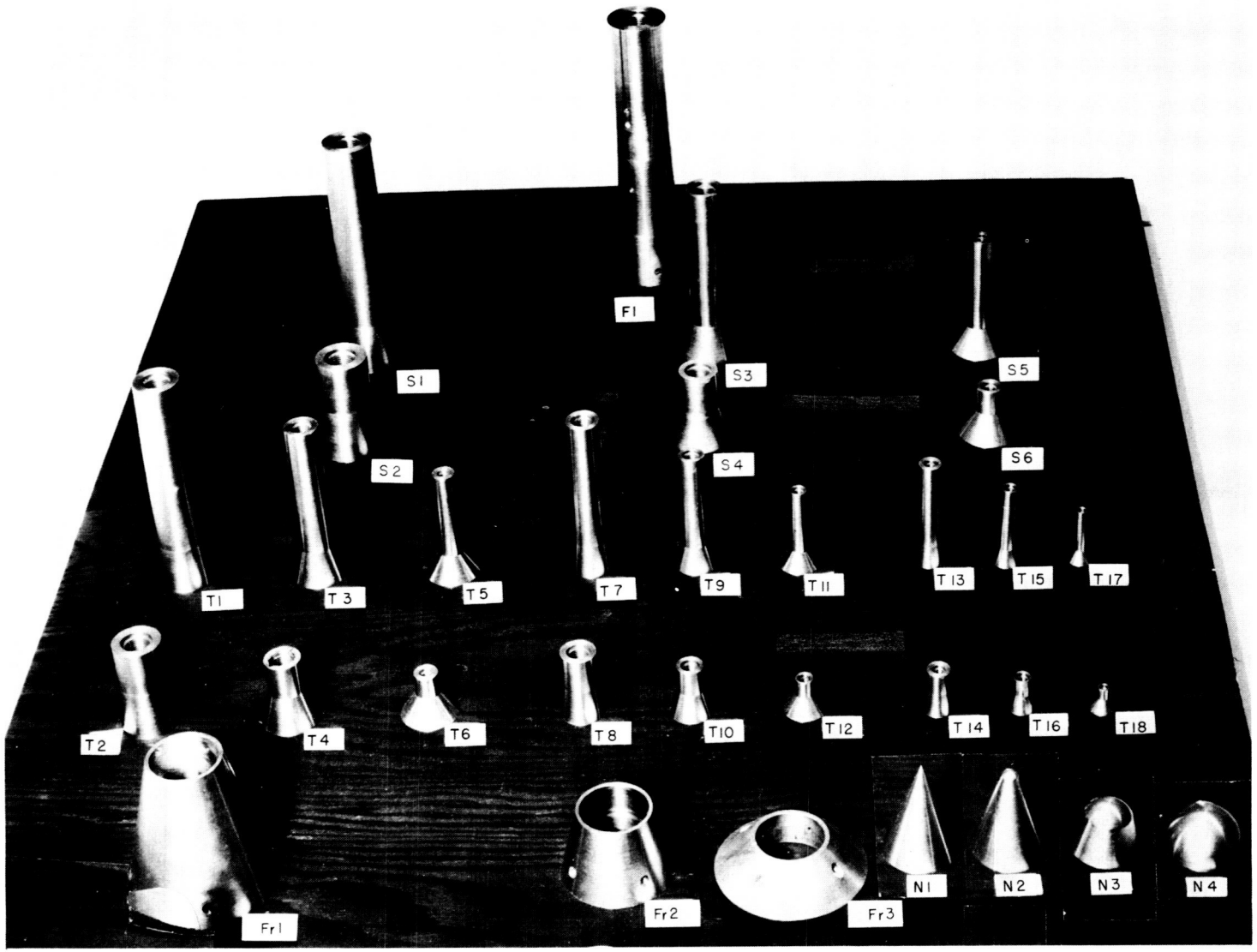

(b) Model components and component designations. L-63-2170.1

Figure 1.- Concluded.

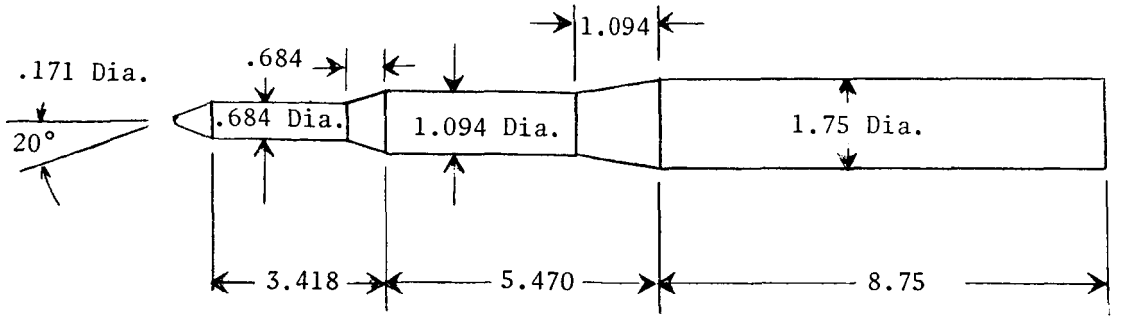

Dimensions of configuration N3-T9-S3-F1

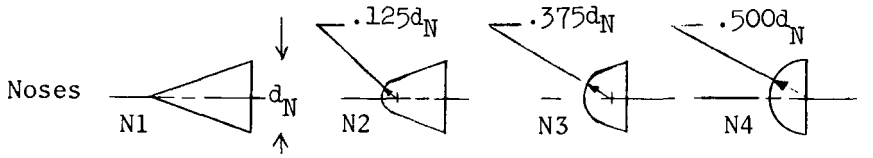

First stage $l_F/d_F = 5$	First- to second-stage diameter ratio, d_F/d_S					
	$l_S/d_S = 2$			$l_S/d_S = 5$		
	1.2 S2	1.6 S4	2.4 S6	1.2 S1	1.6 S3	2.4 S5
Second stage	Second- to third-stage diameter ratio, d_S/d_T					
	$l_T/d_T = 2$			$l_T/d_T = 5$		
S1, S2	1.2 T2	1.6 T4	2.4 T6	1.2 T1	1.6 T3	2.4 T5
S3, S4	T8	T10	T12	T7	T9	T11
S5, S6	T14	T16	T18	T13	T15	T17

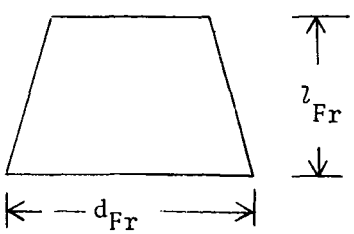

Flares

Config.	d_{Fr}	l_{Fr}	l_{Fr}/d_{Fr}	Half-angle, deg
1	3.500	3.500	1.000	14.0
2	2.625	1.750	.400	14.0
3	3.500	.875	.250	45.0

Figure 2.- Model dimensions and designations. (All dimensions are in inches.)

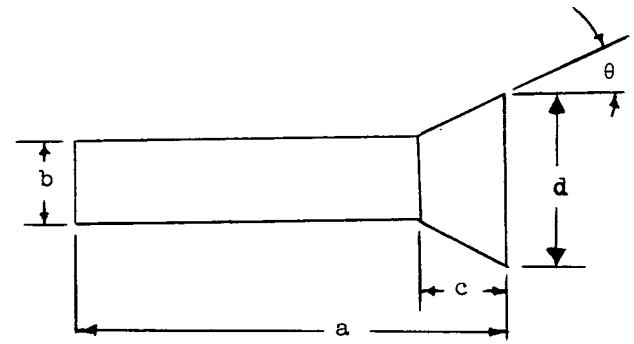

All dimensions in inches

Stage	Total length, a	Stage diameter, b	Flare length, c	Flare diameter, d	Diameter ratio, d/b	Fineness ratio, a/b	Fairing half-angle, θ, deg
F1	8.750	1.750	0		—	5.0	—
S1	7.290	1.458	1.458	1.750	1.2	5.0	5.72
S2	2.916	1.458	1.458	1.750	1.2	2.0	5.72
S3	5.470	1.094	1.094	1.750	1.6	5.0	16.69
S4	2.188	1.094	1.094	1.750	1.6	2.0	16.69
S5	3.645	.729	.728	1.750	2.4	5.0	35.07
S6	1.458	.729	.728	1.750	2.4	2.0	35.07
T1	6.075	1.215	1.215	1.458	1.2	5.0	5.72
T2	2.431	1.215	1.215	1.458	1.2	2.0	5.72
T3	4.557	.911	.911	1.458	1.6	5.0	16.69
T4	1.823	.911	.911	1.458	1.6	2.0	16.69
T5	3.038	.608	.608	1.458	2.4	5.0	35.07
T6	1.215	.608	.608	1.458	2.4	2.0	35.07
T7	4.557	.911	.911	1.094	1.2	5.0	5.72
T8	1.823	.911	.911	1.094	1.2	2.0	5.72
T9	3.418	.684	.684	1.094	1.6	5.0	16.69
T10	1.367	.684	.684	1.094	1.6	2.0	16.69
T11	2.279	.456	.456	1.094	2.4	5.0	35.07
T12	.911	.456	.456	1.094	2.4	2.0	35.07
T13	3.038	.608	.608	.729	1.2	5.0	5.72
T14	1.215	.608	.608	.729	1.2	2.0	5.72
T15	2.279	.456	.456	.729	1.6	5.0	16.69
T16	.911	.456	.456	.729	1.6	2.0	16.69
T17	1.519	.304	.304	.729	2.4	5.0	35.07
T18	.608	.304	.304	.729	2.4	2.0	35.07

Figure 2.- Concluded.

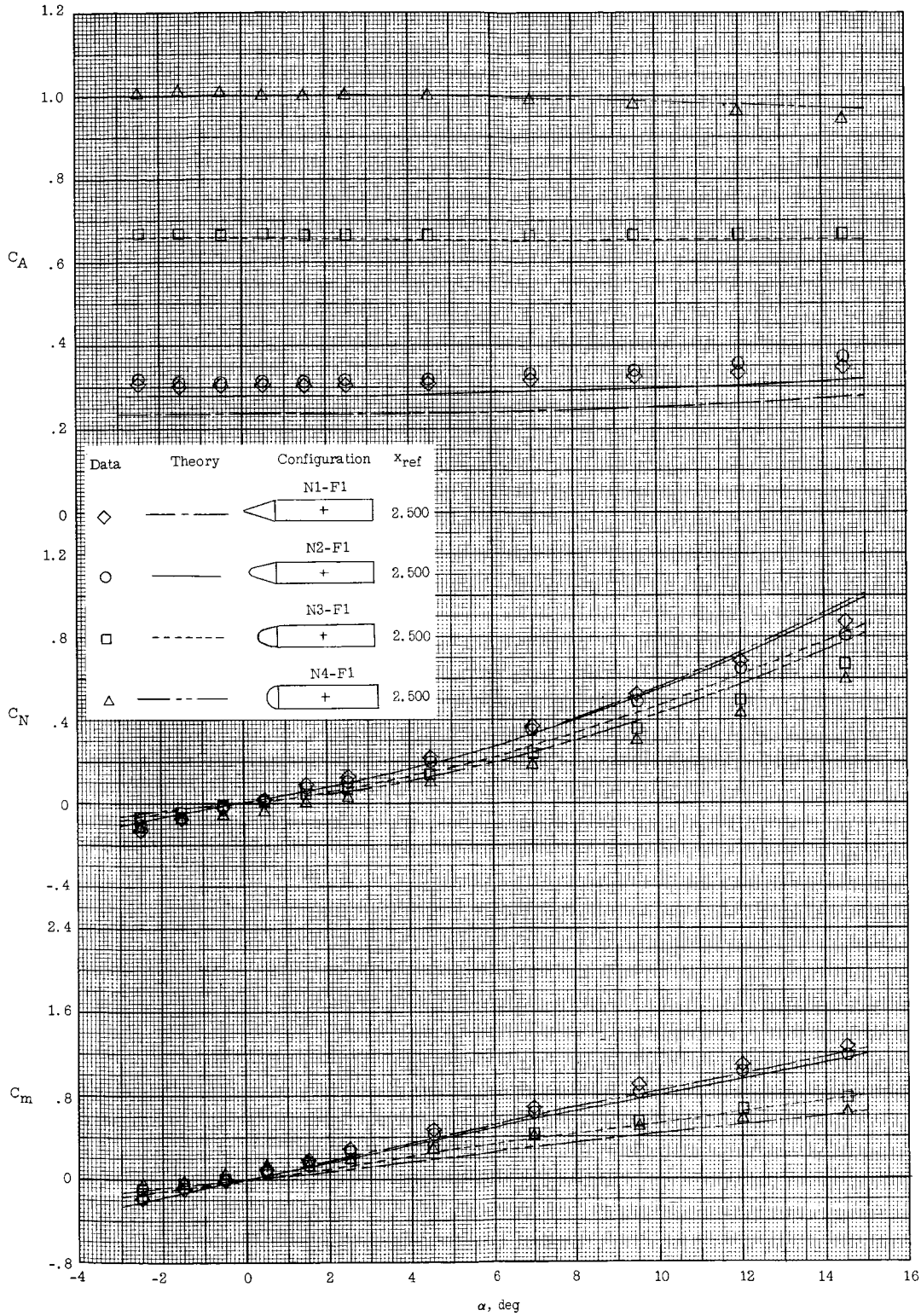

Figure 3.- Effect of nose variation on aerodynamic characteristics of four 1-stage missiles.

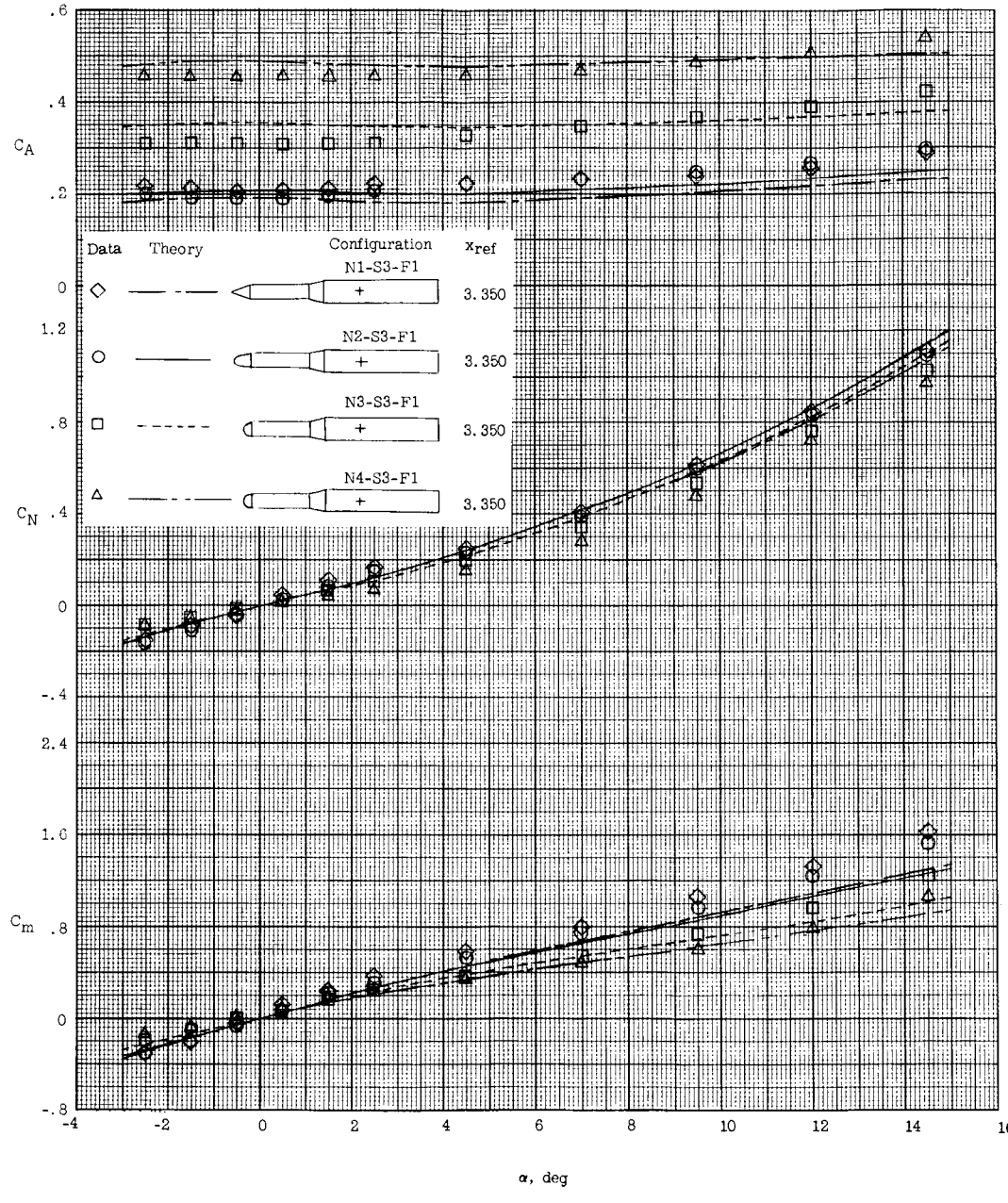

Figure 4.- Effect of nose variation on aerodynamic characteristics of four 2-stage missiles.

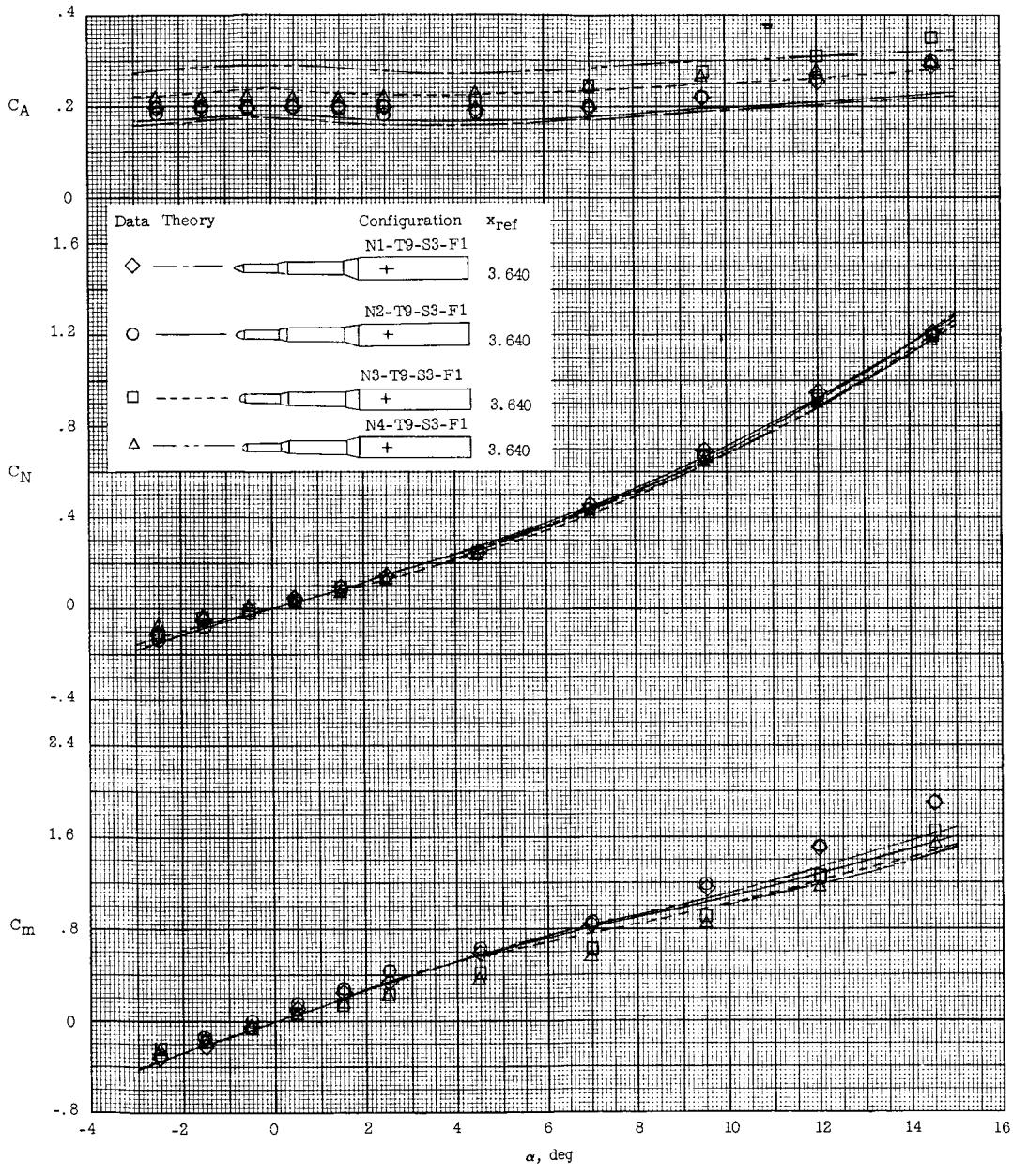

Figure 5.- Effect of nose variation on aerodynamic characteristics of four 3-stage missiles.

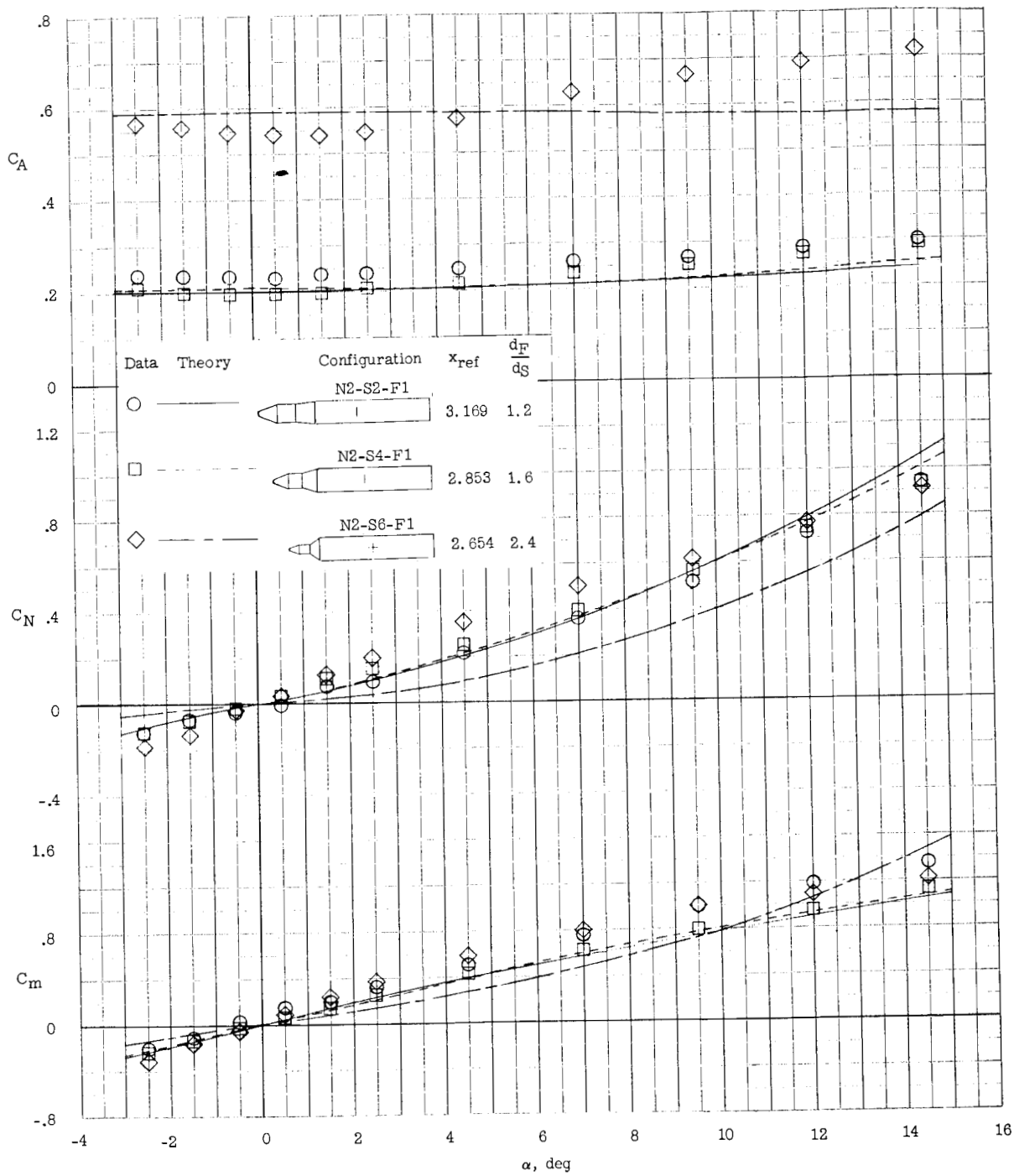

(a) $l_S/d_S = 2.$

Figure 6.- Effect of variation of fineness ratio and interstage diameter ratio on aerodynamic characteristics of six 2-stage missiles.

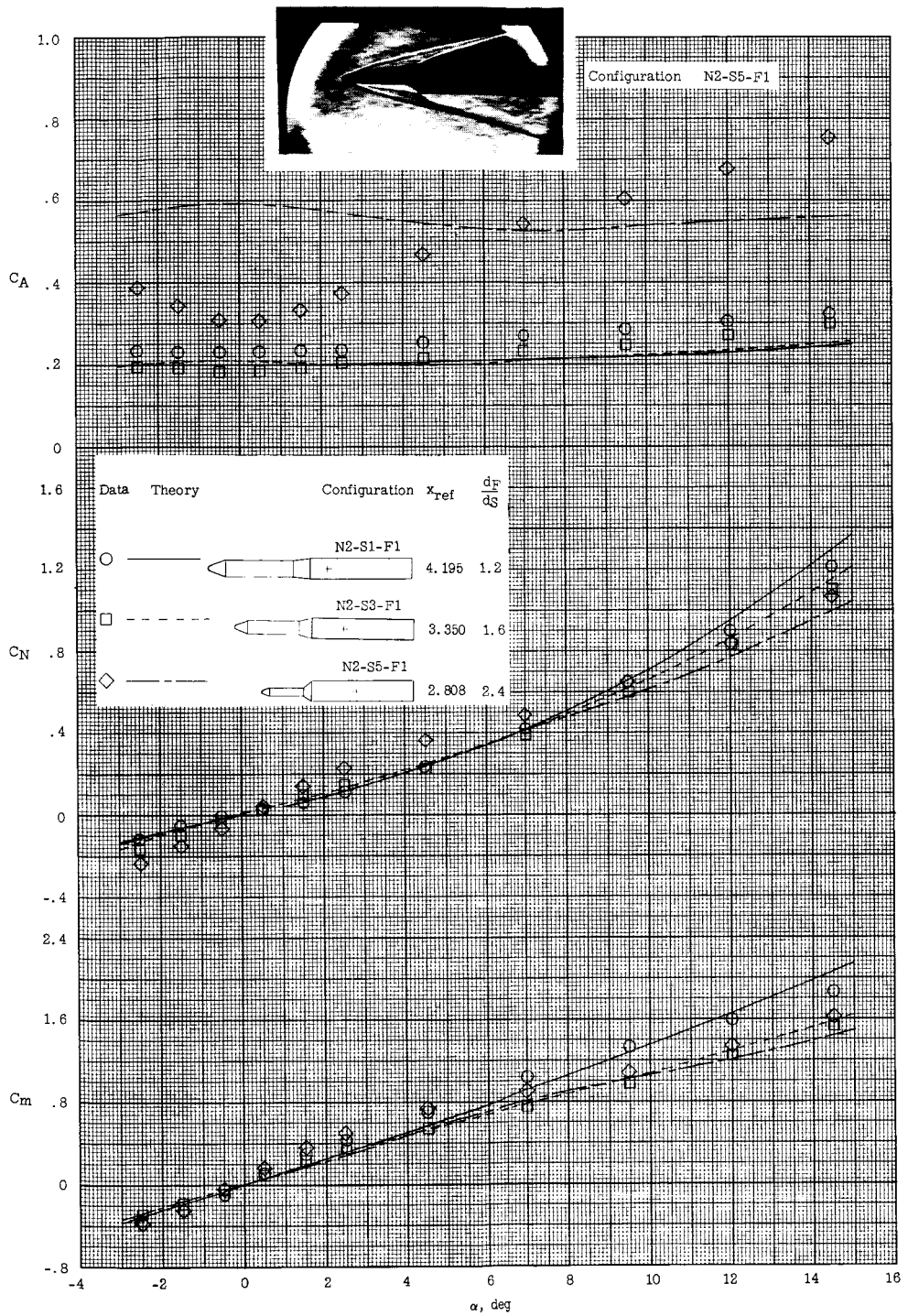

(b) $l_S/d_S = 5.$

Figure 6.- Concluded.

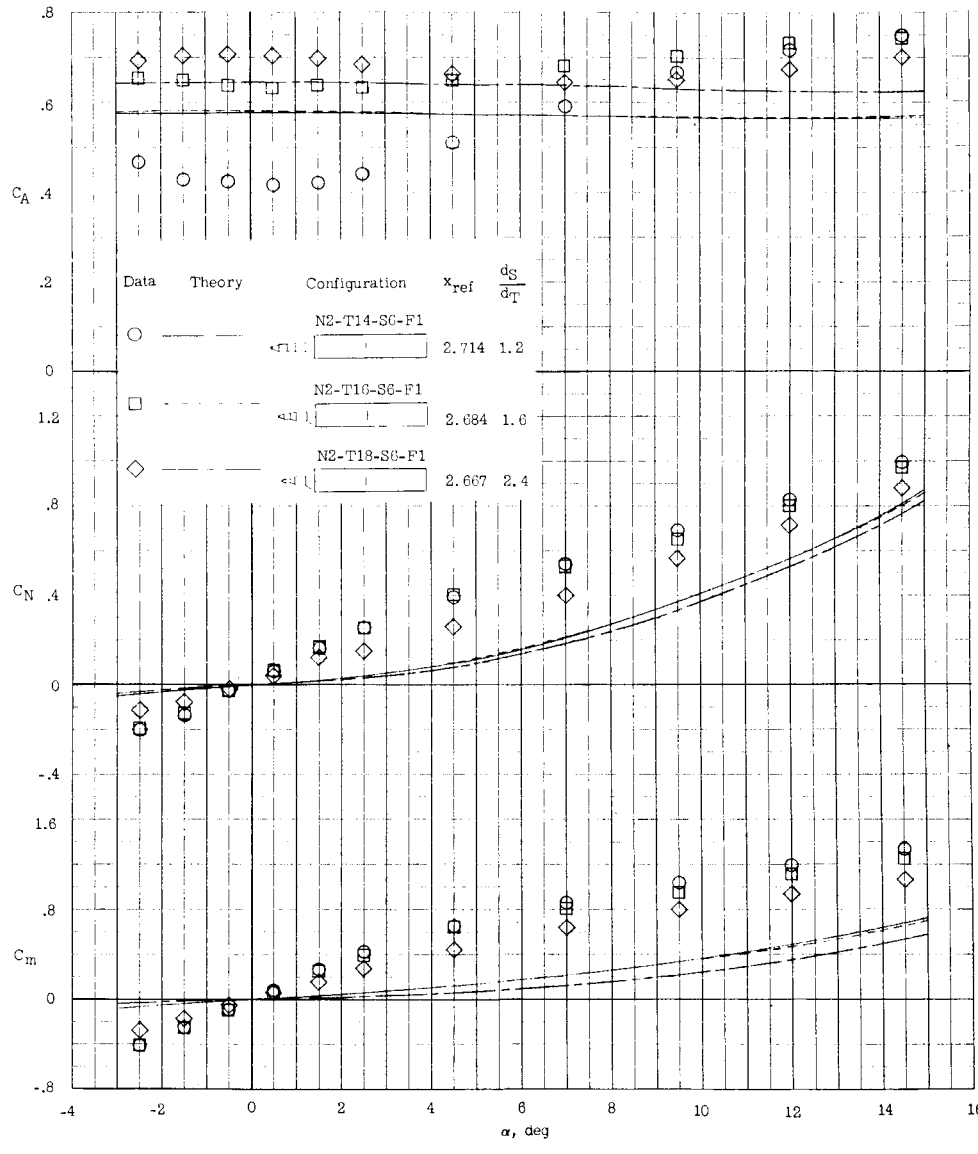

(a) $l_S/d_S = 2$; $l_T/d_T = 2$; $d_F/d_S = 2.4$.

Figure 7.- Effect of variation of fineness ratio and interstage diameter ratio on aerodynamic characteristics of twenty-seven 3-stage missiles.

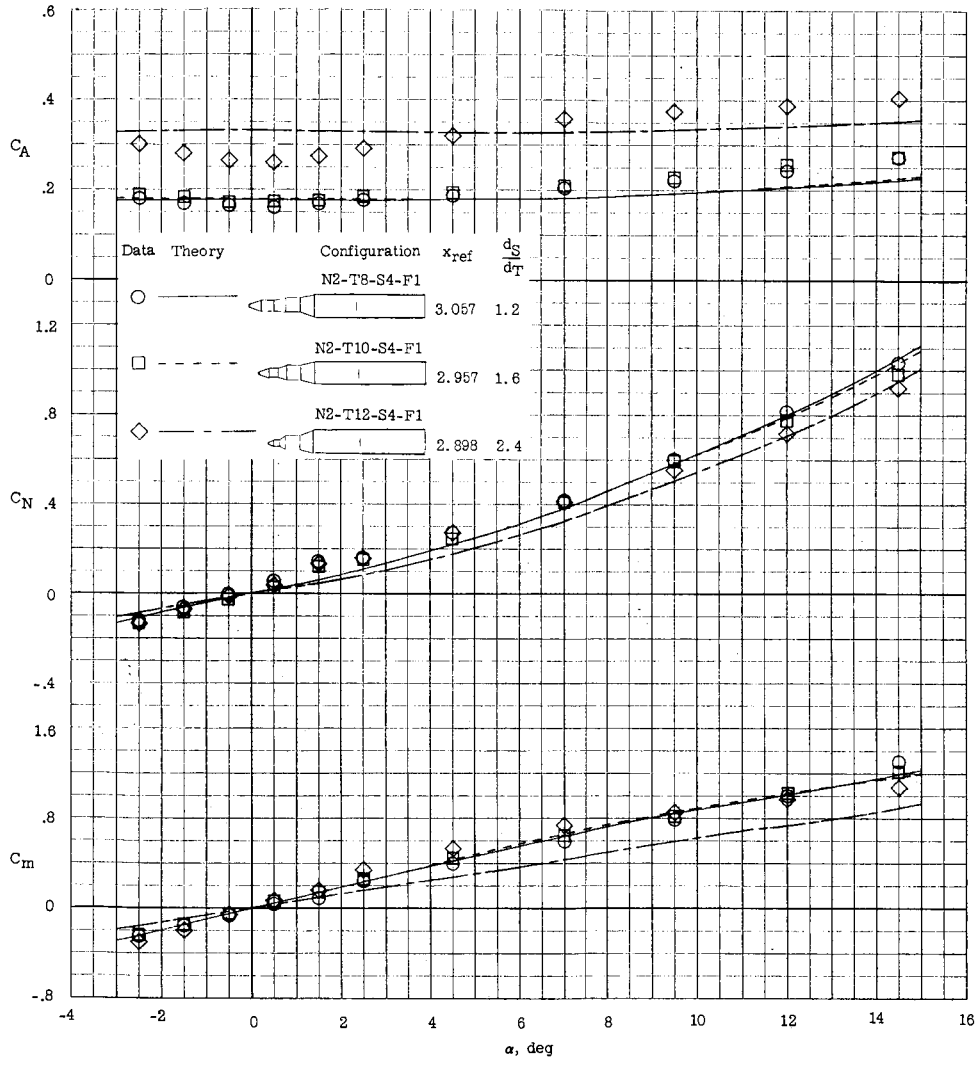

(b) $l_S/d_S = 2$; $l_T/d_T = 2$; $d_F/d_S = 1.6$.

Figure 7.- Continued.

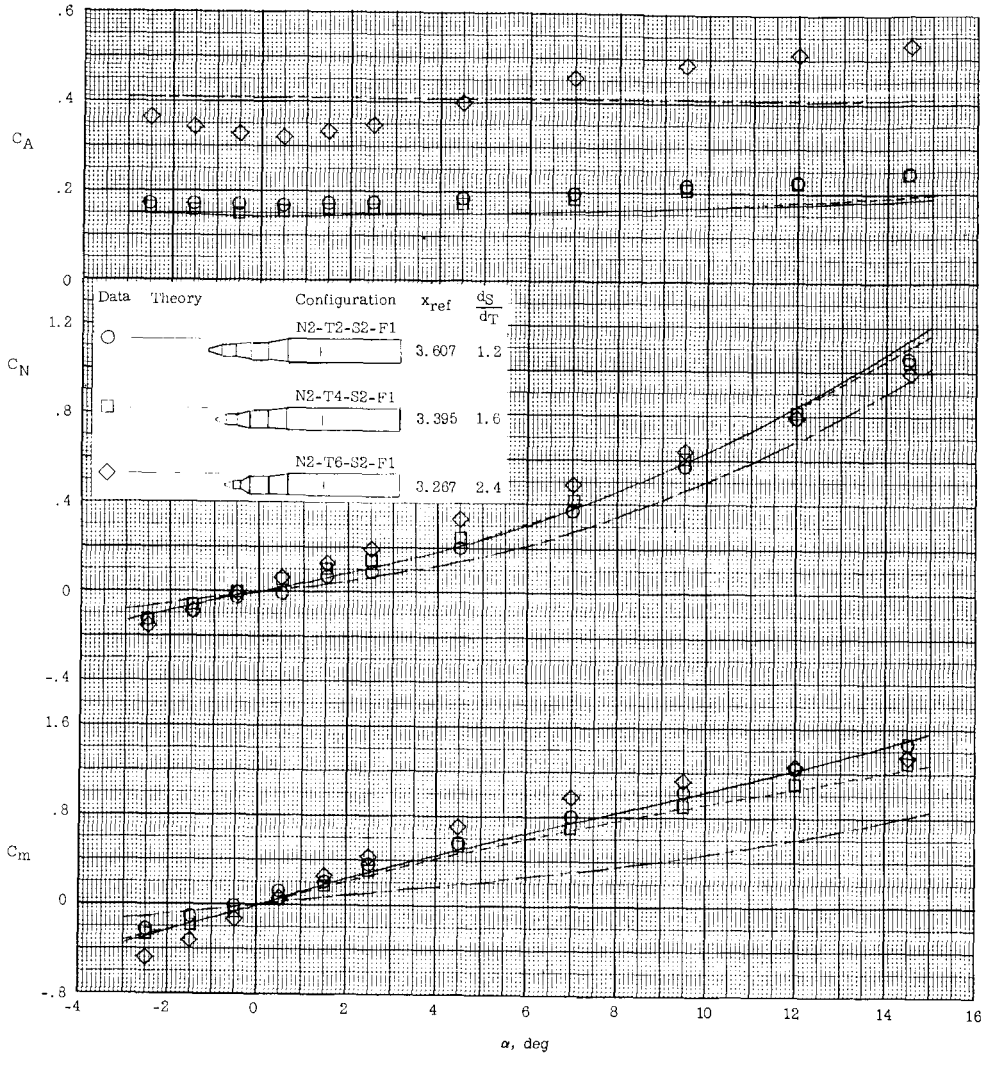

(c) $l_S/d_S = 2$; $l_T/d_T = 2$; $d_F/d_S = 1.2$.

Figure 7.- Continued.

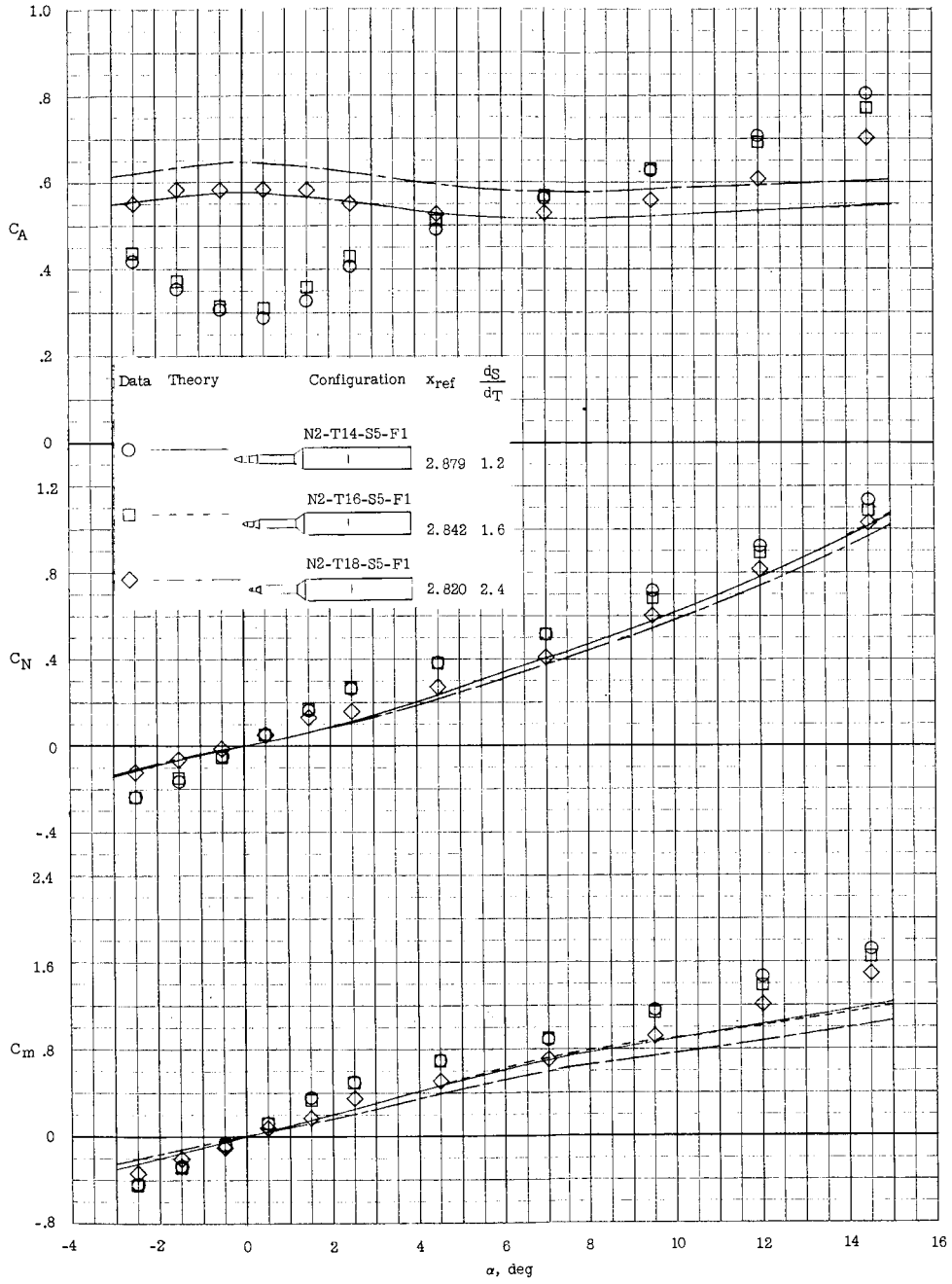

(d) $l_S/d_S = 5$; $l_T/d_T = 2$; $d_F/d_S = 2.4$.

Figure 7.- Continued.

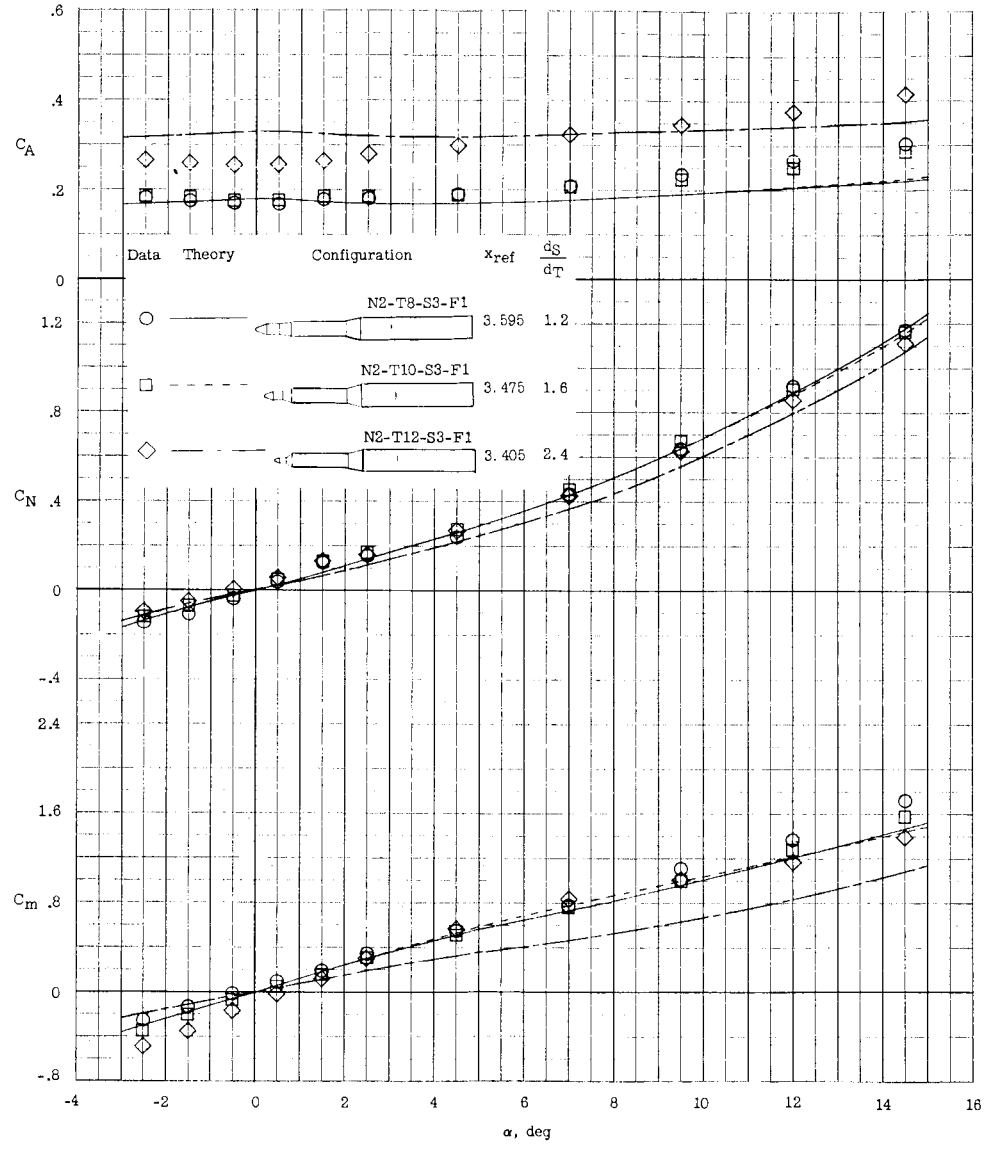

(e) $l_S/d_S = 5$; $l_T/d_T = 2$; $d_F/d_S = 1.6$.

Figure 7.- Continued.

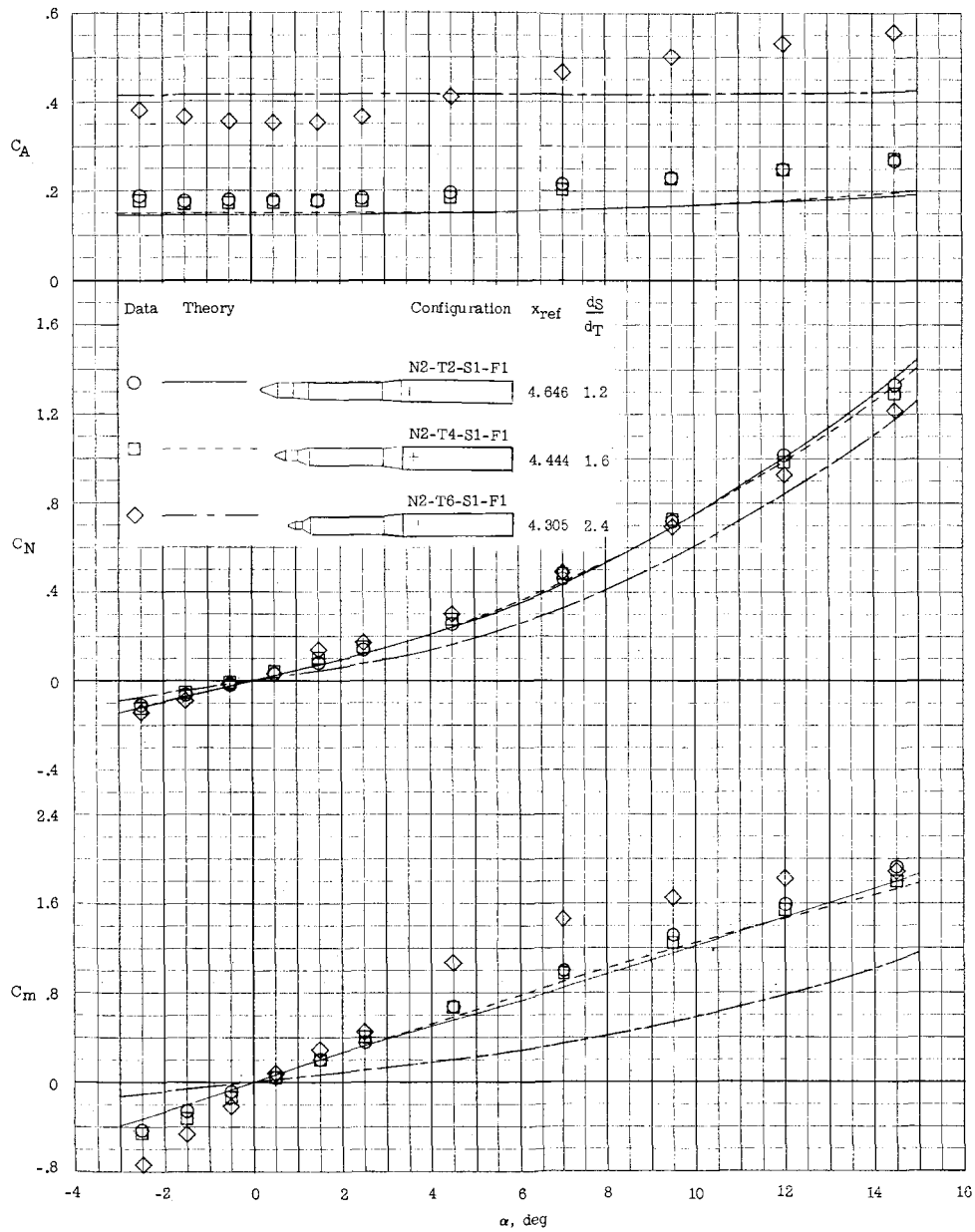

(f) $l_S/d_S = 5$; $l_T/d_T = 2$; $d_F/d_S = 1.2$.

Figure 7.- Continued.

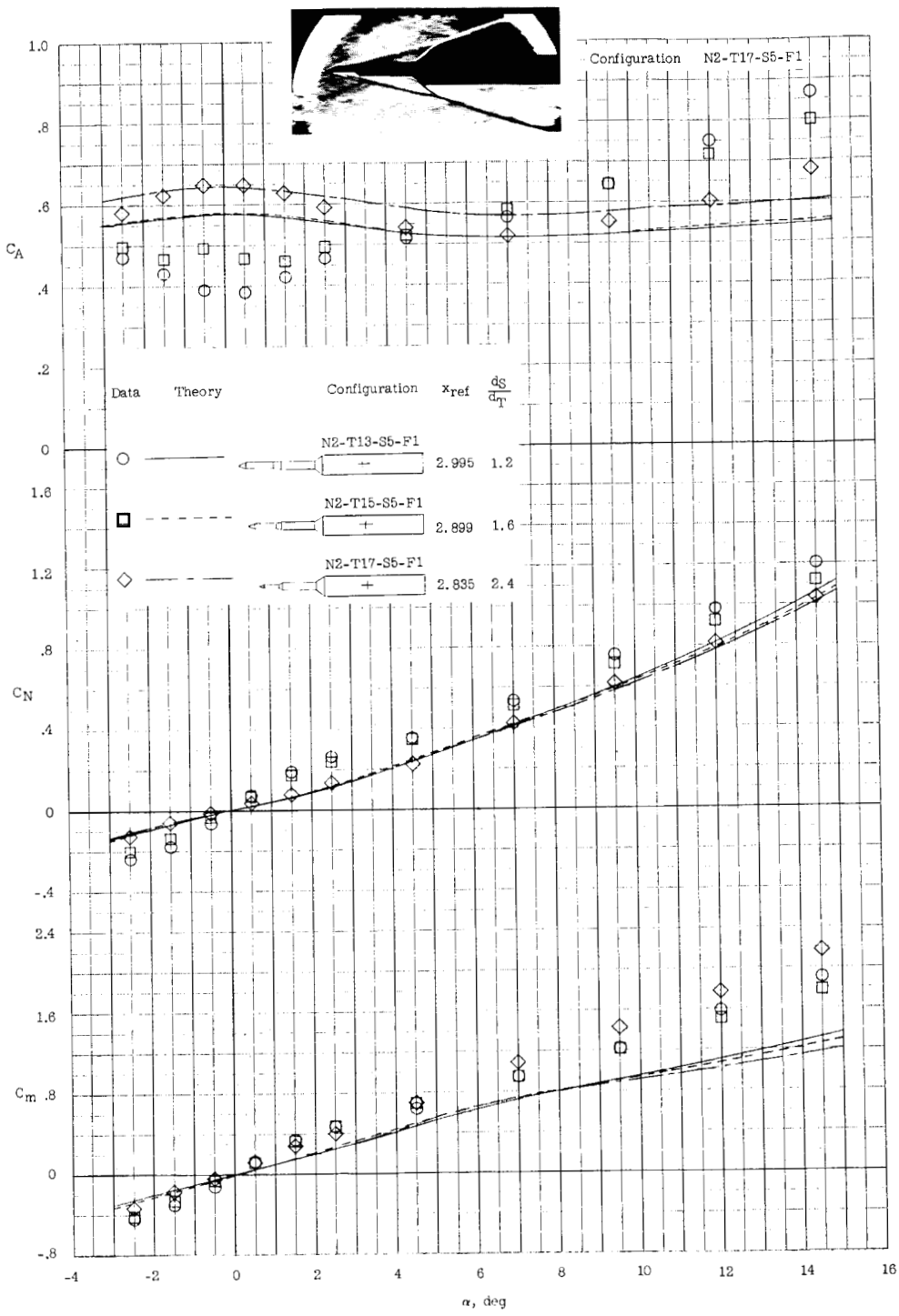

(g) $l_S/d_S = 5$; $l_T/d_T = 5$; $d_F/d_S = 2.4$.

Figure 7.- Continued.

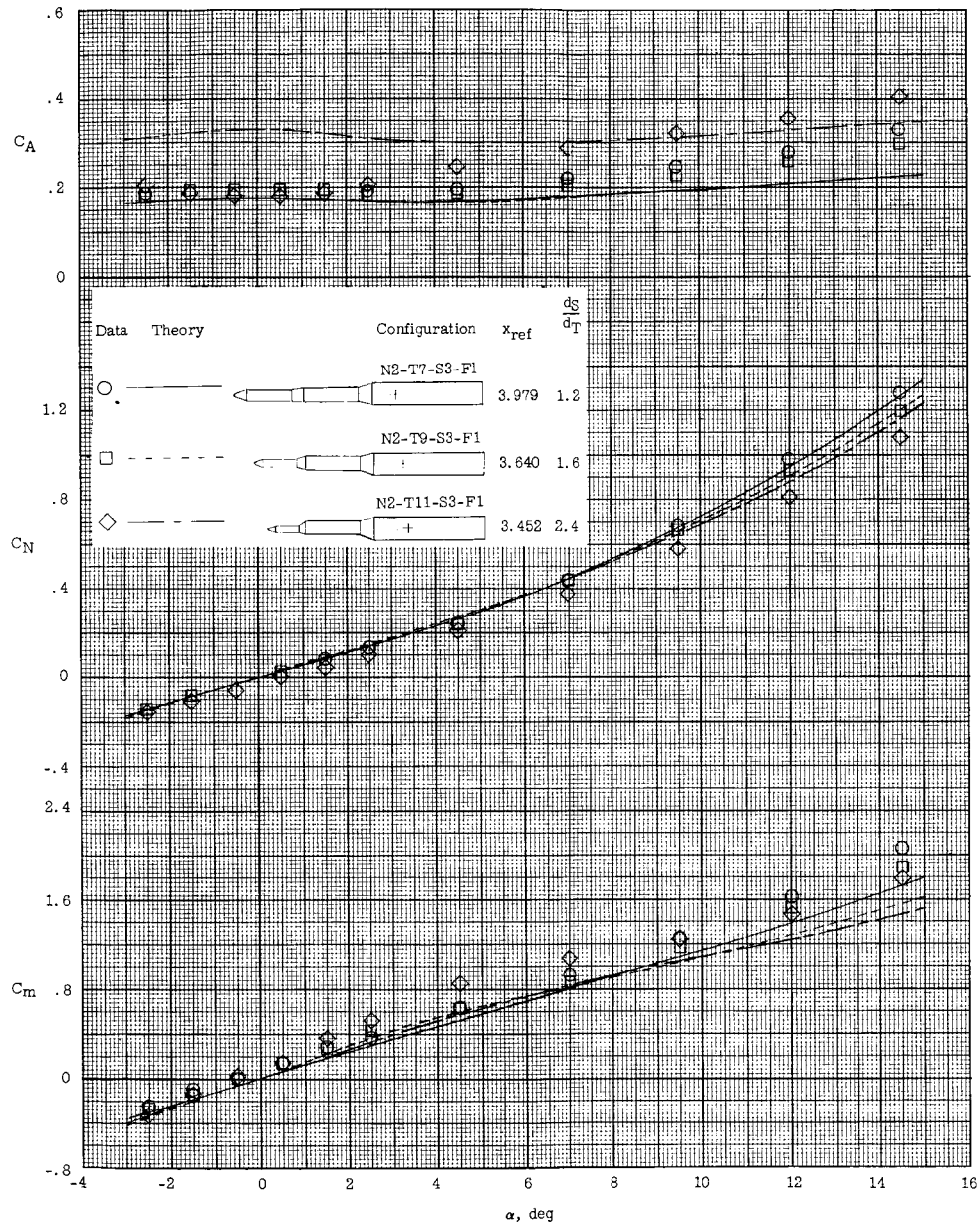

(h) $l_S/d_S = 5$; $l_T/d_T = 5$; $d_F/d_S = 1.6$.

Figure 7.- Continued.

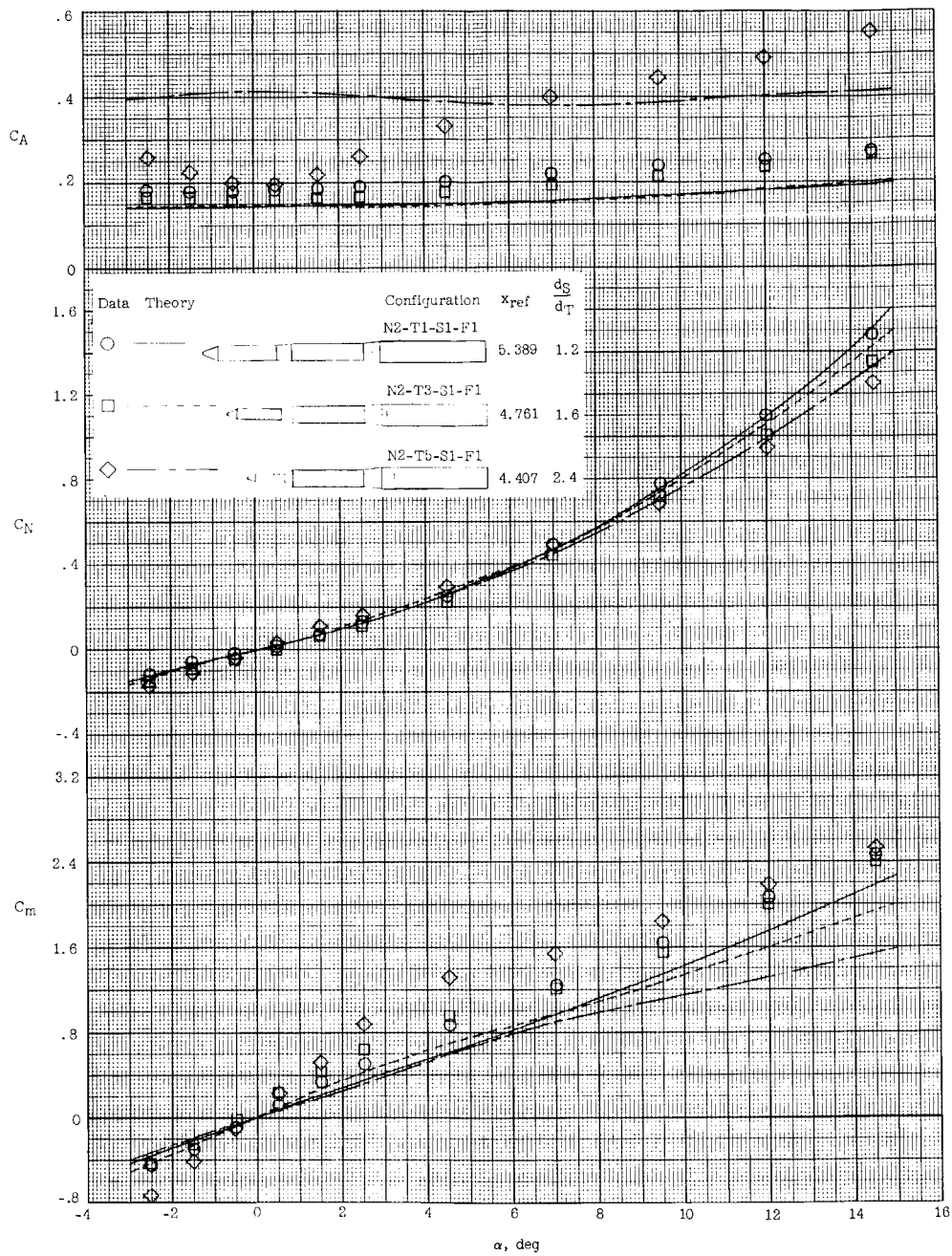

(i) $l_S/d_S = 5$; $l_T/d_T = 5$; $d_F/d_S = 1.2$.

Figure 7.- Concluded.

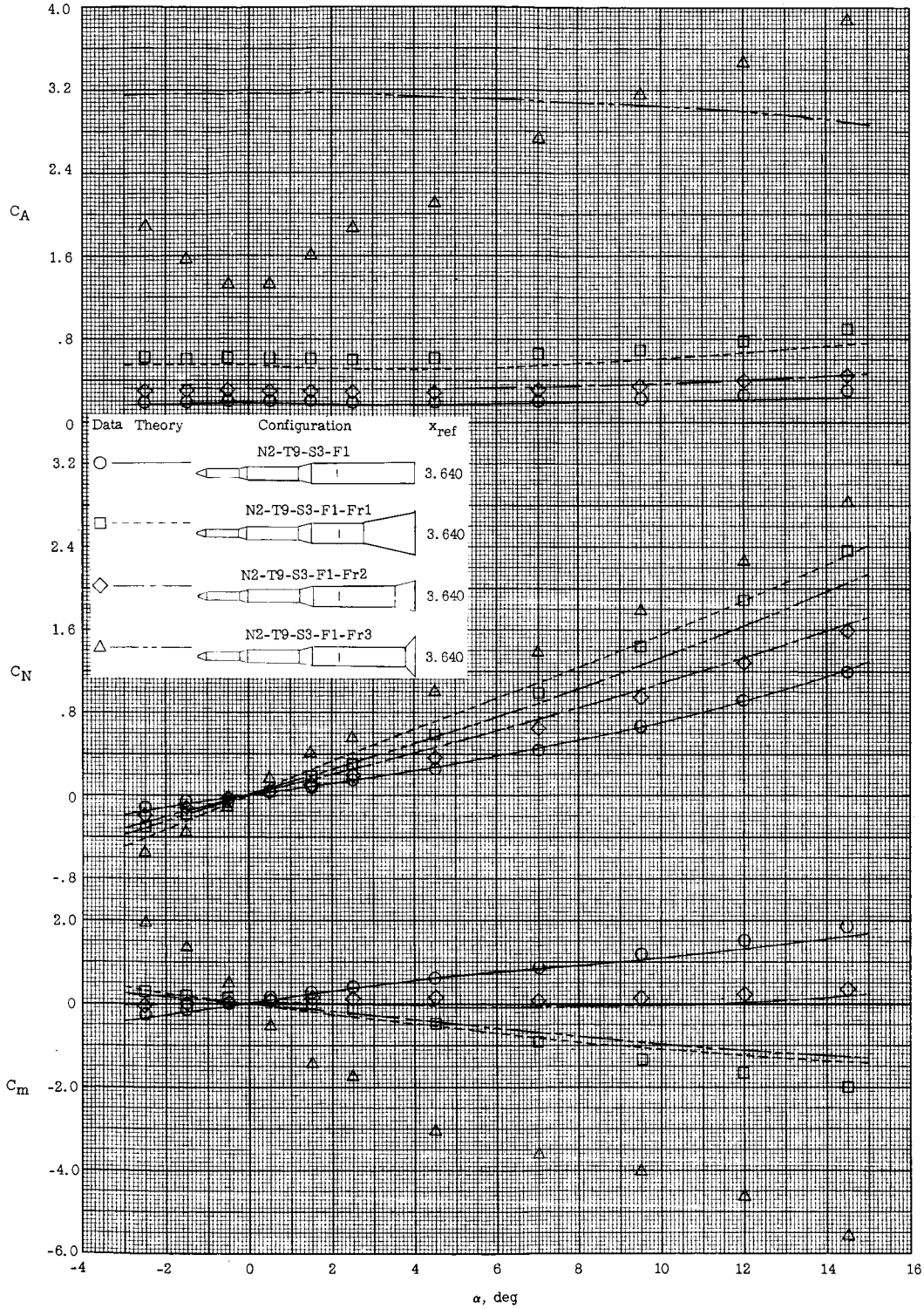

Figure 8.- Effect of various stabilizing flares on aerodynamic characteristics of a typical three-stage configuration.